Journal of Materials Chemistry C

PAPER

View Article Online
View Journal | View Issue

Cite this: J. Mater. Chem. C, 2019, 7, 3634

Impact of molecular conformation on triplet-fusion induced photon energy up-conversion in the absence of exothermic triplet energy transfer†

Hossein Goudarzi,[a] Saurav Limbu,[b] Juan Cabanillas-González,[c] Vassiliki M. Zenonos,[d] Ji-Seon Kim[b] and Panagiotis E. Keivanidis*[d]

The use of photon energy up-converted luminescence driven by triplet-exciton annihilation reactions (TTA-UC) is increasingly gaining attention for developing next-generation light-management, and wavelength-shifting technologies. Here we present a spectroscopic study for elucidating the photophysical mechanism that operates in an unusual TTA-UC model system comprising the blue-light emitting poly(fluorene-2-octyl) (PFO) activator mixed with the green-light absorbing (2,3,7,8,12,13,17,18-octaethyl-porphyrinato) Pt^{II} (PtOEP) metalo-organic complex. The unconventional character of the PFO:PtOEP composite manifests in the fact that no exothermic triplet energy transfer (TET) is possible between triplet-excited PtOEP and PFO. Yet green-to-blue TTA-UC luminescence of PFO is obtained even when PtOEP is selectively photoexcited by pulsed laser intensities as low as 2.5 mW cm^{-2}. Continuous-wave photo-induced absorption spectroscopy verifies that no energy transfer from triplet-excited PtOEP to the triplet level of PFO takes place, pointing to triplet–triplet annihilation (TTA) events in the PtOEP phase as the origin of the observed TTA-UC PL signal. In the PFO:PtOEP composite, the PtOEP component holds a dual role of annihilator/sensitizer; photon energy storage in PtOEP is enabled *via* TTA when triplet exciton diffusion coefficient values of D_{PtOEP} = 4.1 × 10^{-9} cm^2 s^{-1} are reached. With a simple yet powerful solution processing protocol, and by combining Raman and time-gate photoluminescence (PL) spectroscopy we demonstrate that the brightness of the produced TTA-UC luminescence depends on the molecular conformation of the PFO activator. A four-fold increase in the TTA-UC luminescence intensity is registered in the time-integrated and time-gated PL spectra, when the PFO matrix is arrested in its planar β-phase molecular conformation. Further enhancement of the TTA-UC PL signal is achieved when temperature lowers from 290 K down to 100 K. These results stimulate the development of a theoretical model for the microscopic description of triplet exciton migration in disordered photon up-converting solids. Efficient harvesting of photon energy, which is stored in annihilator/sensitizer moieties *via* TTA events, can be enabled when the molecular conformation of the activator species is properly tuned.

Received 13th December 2018,
Accepted 25th February 2019

DOI: 10.1039/c8tc06283h

rsc.li/materials-c

Introduction

Triplet–triplet exciton annihilation (TTA) is a well-studied photophysical process in organic material systems that is driven by the fusion of triplet excited states, leading to the generation of delayed fluorescence; that is emission of light with a characteristic spectral shape similar to that of fluorescence albeit with a longer emission lifetime.[1–3] An intriguing manifestation of this type of delayed luminescence is the detection of TTA-induced photon up-converted (TTA-UC) light emission that is observed at wavelengths shorter than the photoexcitation wavelength used.[4] Essentially, the key-step in the TTA-UC process is the selective photoexcitation of a triplet sensitizer in a sensitizer:activator blend by low photon energy

[a] Centre for Nano Science and Technology@PoliMi, Fondazione Istituto Italiano di Tecnologia, Via Pascoli 70/3, 20133 Milano, Italy
[b] Imperial College London, Blackett Laboratory, Prince Consort Road, London SW7 2AZ, UK
[c] Fundacion IMDEA Nanociencia, Ciudad Universitaria de Cantoblanco, Calle Faraday 9, Madrid, ES 28049, Spain
[d] Department of Mechanical Engineering and Materials Science and Engineering, Cyprus University of Technology, Limassol 3041, Cyprus. E-mail: p.keivanidis@cut.ac.cy

† Electronic supplementary information (ESI) available: Tabled Raman data, time-integrated PL spectra of PFO-only, PFO:PtOEP and PS:PtOEP films, time-gated TTA-UC PL kinetics of PFO:PtOEP and PF26:PtOEP films, time-gated PL spectra of PS:PtOEP and PFO:PtOEP films, atomic force microscopy images of PS:PtOEP and PFO:PtOEP films. See DOI: 10.1039/c8tc06283h

radiation that triggers an exothermic triplet energy transfer from the sensitizer to the activator.[5–7] Following an efficient triplet energy transfer (TET) step a reservoir of triplet excited-state activators is prepared that facilitates TTA reactions between activators and generates TTA-UC delayed luminescence. The established model system of this type of TTA-UC composites is based on the combination of the green-absorbing metallo-organic triplet sensitizers such as (2,3,7,8,12,13,17,18-octaethyl-porphyrinato) Pt^{II} (PtOEP) or (2,3,7,8,12,13,17,18-octaethyl-porphyrinato) Pd^{II} (PdOEP) mixed with the blue-emitting di-phenyl anthracene (DPA) activator, in which the triplet excited state of the sensitizer is energetically higher than the triplet excited state of DPA.[8,9] Notably, in this class of photon up-converters the DPA activator molecules hold a dual role of annihilation/emitter.[10]

For most of the technologically important applications the development of solid-state TTA-UC schemes is sought,[11] however the fabrication of high performance TTA-UC composite films is difficult to achieve and the TTA-UC photoluminescence quantum yield (PLQY) remains low in the order of 1–4%.[12–14] The main bottleneck that impedes high efficiency TTA-UC luminescence comes from the high strength of excitonic coupling effects due to enhanced intermolecular interactions of the composite components in the solid state. In particular, the aggregation of the PtOEP triplet sensitizer[15,16] results in the formation of PtOEP dimer states that act as energy-scavengers and funnel energy back to the ground state, thereby limiting the efficiency of the required TET step. Most importantly, PtOEP aggregates facilitate unwanted TTA events between triplet-excited PtOEP pairs that further waste the stored photon energy in PtOEP. Parasitic TTA events in the PtOEP phase can become so severe, manifesting in the detection of TTA-induced delayed PtOEP fluorescence in the ns time scale, even when photoexcitation intensities in the order of mW cm^{-2} are used.[17]

A smart approach to exploit the tendency of triplet-excited sensitizer species to undergo TTA reactions in the solid state is to employ them as annihilator/sensitizer components in TTA-UC composites. As Fig. 1 depicts, the annihilation of triplet-excited PtOEP sensitizers prior to any TET step results in the population of a doubly photoexcited PtOEP state that can potentially facilitate energy- or charge transfer to an activator and induce TTA-UC. This rather unconventional TTA-UC excited state pathway has been identified by earlier TTA-UC studies of polymeric composites comprising blue-light emitting poly(*para*-phenylene)-type activators such as poly(fluorene) (PF) mixed with PtOEP.[18–20] In those systems, green-to-blue TTA-UC luminescence generation is detectable although no exothermic triplet energy transfer step from PtOEP to PF is energetically allowed; the first triplet excited state of the PtOEP sensitizer (T_{1_PtOEP} = 1.92 eV) is energetically placed well-below the first triplet excited state of PF, rendering the properties of the triplet excitonic states in the polymer irrelevant to the particular type of TTA-UC. Yet, in recent literature[21,22] the generation of green-to-blue TTA-UC luminescence by the binary PF:PtOEP system is believed to originate by the fusion of PFO triplet excitons formed after TET from PtOEP to PF. This misconception has impeded the full elucidation of this type of TTA-UC luminescence, and little attention[8,23,24] has been given to the TTA-UC photophysics of unconventional up-converting composites. To this date the nature of the TTA-induced doubly photoexcited PtOEP state remains elusive with transient absorption studies to suggest that it corresponds to a metal-centered (d–d) excited state.[25] In addition, the experimental observation of delayed PtOEP fluorescence[17] in solid films of the metallo-organic PtOEP complex verifies that TTA reactions between triplet-excited PtOEP species indeed activate a higher lying PtOEP excited level. Therefore, an alternative excited state route seems to be realistically available for the pooling of photon energy that can be effectively used in driving the sensitization of dye-sensitized solar cells, luminescent probes, photocatalysts, electrochemical devices and photonics switches.

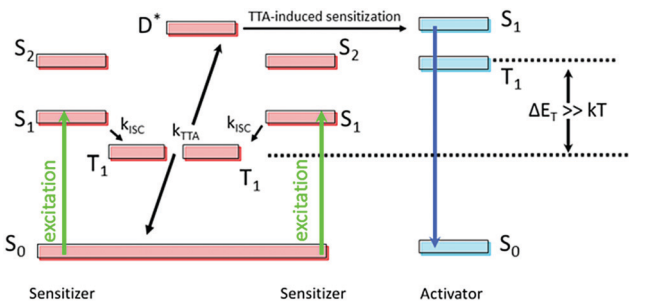

Fig. 1 Triplet–triplet-annihilation-induced photon energy up-conversion in unconventional composites where no exothermic triplet energy transfer from sensitizer to activator is energetically probable. Triplet–triplet annihilation between triplet-excited sensitizers is followed by energy transfer from a doubly photoexcited sensitizer state (D*) to a nearby activator that exhibits TTA-UC luminescence. In this scheme the low-energy photon absorber holds a dual annihilator/sensitizer role that drives the sensitization of a high-photon energy emitting activator.

Early photokinetic studies of thin films[23] and solutions[26] have independently suggested that the generation of TTA-UC luminescence by unconventional composites involves the participation of sensitizer/activator co-aggregates. The derived binding constant of the proposed co-aggregates are in the order of 10^{-1} M^{-1}. That is significantly lower than the typical value expected for adducts formed in solutions by the coordination of an emitter to the axial position of the octaethylporphyrin sensitizer,[27] hence manifesting the weak driving force for co-aggregate formation that impedes direct experimental verification. More recently, electro-optical studies on this type of TTA-UC systems demonstrated the quenching of the TTA-UC luminescence by an externally applied electric field,[24,28] thus suggesting that an electron-exchange-based energy transfer mechanism drives the TTA-UC through a transient charge transfer state formed between the doubly photoexcited sensitizer and the ground state activator. Another observation that agrees empirically with the proposed mechanism is the detection of a relatively stronger up-converted luminescence by highly planarized ladder type poly(*para*-phenylene) derivatives in respect to poly(fluorene)-based emitters that have a broader conformer distribution.[19,24] For that reason, one should expect that the molecular conformation of the participating species strongly

dictates the strength of the produced TTA-UC luminescence. Within this context, the optimization of the activator molecular conformation can become a major engineering tool for achieving optimum molecular orbital overlap between the sensitizer/activator couple. Molecular conformation influences the phosphorescence properties of organic emitters.[29] Nonetheless, a study that directly addresses the impact of molecular conformation on the up-converted luminescence generation in this class of TTA-UC systems is still lacking.

Here we directly address the effect of the activator molecular conformation on the overall TTA-UC performance of unconventional solid-state polymeric TTA-UC composites. For our work we employ solid-state composite films of the poly(fluorene-2-octyl) (PFO) activator mixed with the triplet sensitizer PtOEP. In these films the PFO derivative can be arrested in two distinct molecular conformations; the glassy amorphous α-phase and the β-phase.[30] The latter corresponds to a specific molecular conformation of the PFO chains that adapt a rigid, chain-extended structure with an inter-monomer torsion angle of about 180°, such that the octyl-substituents of neighboring fluorene units lie on alternating sides of the PFO polymer backbone. Each of the two distinct molecular PFO conformations exhibit characteristic UV-Vis absorption features and photoluminescence (PL) spectral patterns; the β-phase PFO manifests by a unique absorption peak at around 435 nm in its UV-Vis absorption spectrum while in its fluorescence spectrum the $S_{0\text{–}0} \leftarrow S_{1\text{–}0}$ radiative transition peaks at around ~440 nm, which is red-shifted in comparison to the corresponding $S_{0\text{–}0} \leftarrow S_{1\text{–}0}$ PL peak of the PFO α-phase that centers at ~420 nm. Accordingly, the first triplet excited state T_1 of the β-phase for PFO is energetically lower ($T_{1\_PFO\text{-}\beta}$ = 2.08 eV) than the corresponding first triplet excited state of the α-phase ($T_{1\_PFO\text{-}\alpha}$ = 2.15 eV).[31] For our work, we adapt a simple yet powerful solution-processing protocol[17] for systematically tuning the planarity of the PFO matrix and we demonstrate a nearly four-fold increase in the TTA-UC luminescence intensity of PFO:PtOEP thin films when a highly planar molecular conformation of the PFO activator is achieved. The absence of a TET step from triplet-excited PtOEP to PFO in the studied films is verified by continuous-wave photo-induced absorption (cw-PIA) experiments. For reference purposes, the spectroscopic properties of poly(styrene) (PS):PtOEP and poly(fluorene-2-ethyl-hexyl) PF26:PtOEP blend films are also studied.

Results and discussion

Fig. 2a presents the molecular structures of PtOEP, PF26 and PFO. For tuning the backbone planarity of the PFO matrix in

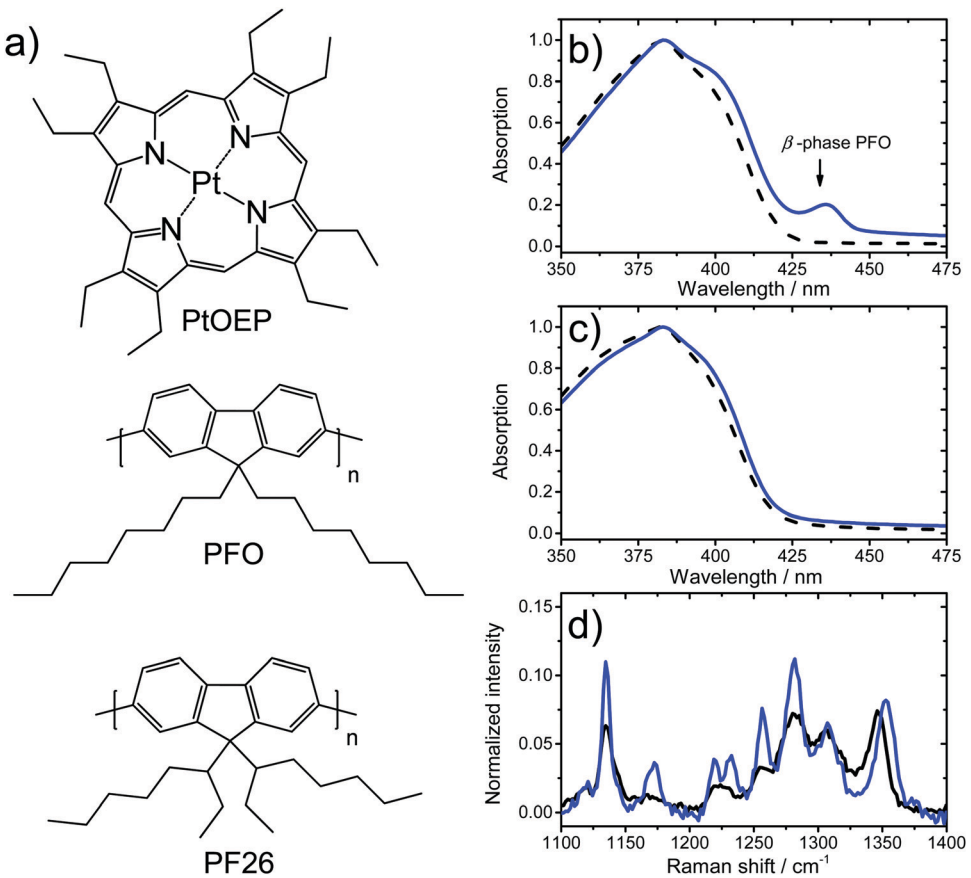

Fig. 2 (a) The chemical structures of the annihilator/sensitizer (PtOEP) and activator (PFO and PF26) materials used in this study, (b) UV-Vis absorption spectra of PFO:PtOEP 6 wt% films spun from chloroform (black dash line) and toluene (blue solid line), (c) UV-Vis absorption spectra of PF26:PtOEP 6 wt% films spun from chloroform (black dash line) and toluene (blue solid line), (d) normalized Raman spectra of PFO:PtOEP 6 wt% films spun from chloroform (black line) and toluene (blue line).

the studied blends, chloroform and toluene are used as processing solvents due to the large difference in their boiling points, and their wide availability in most of the optical spectroscopy laboratories. Fig. 2b presents the UV-Vis spectra of the PFO:PtOEP 6 wt% films focusing in the spectral region of 350–475 nm where the appearance of the characteristic PFO β-phase absorption peak at 435 nm is expected.

Clearly, only the PFO:PtOEP 6 wt% film developed by toluene exhibits the spectral signature of the PFO β-phase that co-exists with the absorption peak of the PFO α-phase. The latter is found superimposed on the PtOEP Soret absorption band in the spectral region of 380–400 nm. In contrast, no spectral signature of the PFO β-phase absorption peak is found in the PFO:PtOEP 6 wt% film developed by chloroform. As expected, the relatively lower boiling point of chloroform facilitates the faster evaporation of the solvent during spin-coating, thereby arresting the PFO chains in the molecular conformation of the kinetically entrapped glassy α-phase.[32] We have performed the same UV-Vis characterization experiment in a set of two PF26:PtOEP 6 wt% films developed by toluene and chloroform. Fig. 2c shows that the UV-Vis spectra of these two films are identical confirming that no chain conformation corresponding to the β-phase is possible for the PF derivative functionalized with ethyl-hexyl-side chains, regardless of the boiling point of the solvent used. We have further collected Raman spectroscopic data for the two PFO:PtOEP 6 wt% blend films developed by chloroform and toluene. Fig. 2d presents Raman spectra of these two systems after photoexcitation of the films at 457 nm and normalized at 1600 cm^{-1}, in the spectral region where the strong Raman peak due to symmetric stretch of phenylene rings in the fluorene monomer is observed. Detailed indexing of the Raman data is provided in the ESI.† For clarity, only the spectral region of 1100–1400 cm^{-1} is shown that corresponds to the vibrational modes of the PFO backbone[33–35] and where the Raman signature of the PFO β-phase is expected. Compared to the chloroform cast film, the film developed by toluene exhibits sharper and higher relative intensity of Raman peaks in the spectral region of 1100–1400 cm^{-1} (with respect to peak at 1600 cm^{-1}), which is characteristic of higher PFO β-phase.[36] Thus, in agreement with the UV-Vis results, the obtained data verify the formation of a higher β-phase PFO conformers concentration in PFO:PtOEP 6 wt% film developed by toluene.

Next, we performed PL characterization measurements for both sets of PFO:PtOEP 6 wt% and PF26:PtOEP 6 wt% blend films developed by chloroform and toluene. For this purpose, the films were photoexcited in resonance with the Q-absorption band of PtOEP at 532 nm (see ESI†), where the PF matrices do not absorb. Fig. 3a presents the normalized time-gated PL spectra of the PFO:PtOEP 6 wt% and PF26:PtOEP 6 wt% blend films developed by chloroform, whereas the normalized time-gated PL spectra of the PFO:PtOEP 6 wt% and PF26:PtOEP 6 wt% blend films spun from toluene are shown in Fig. 3b.

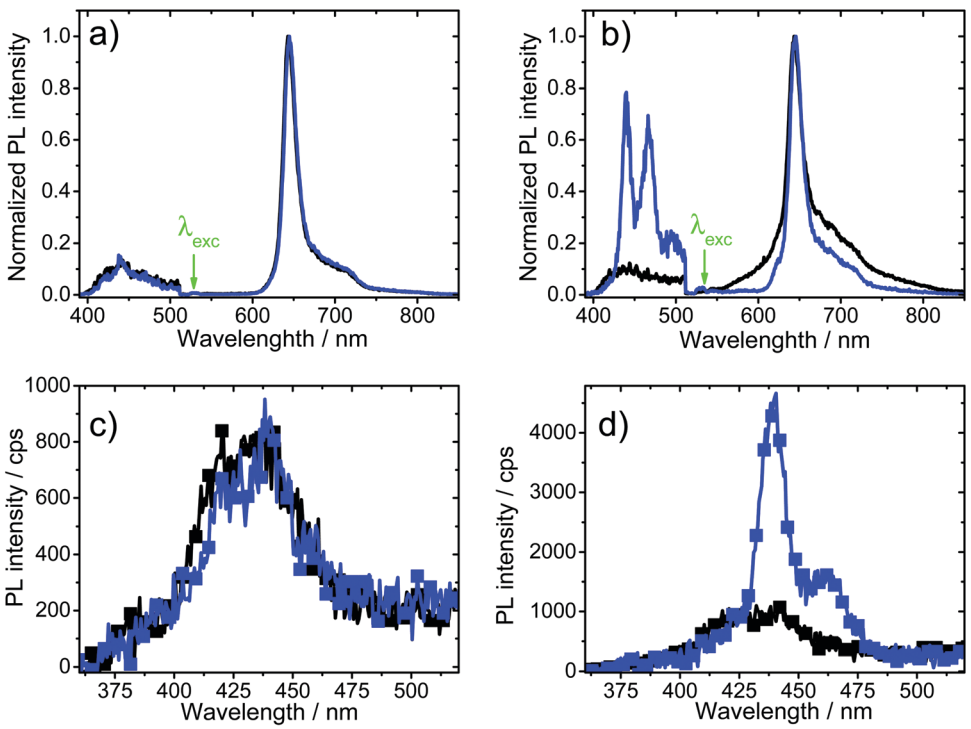

Fig. 3 Normalized time-gated PL spectra of PF26:PtOEP 6 wt% (black lines) and PFO:PtOEP 6 wt% (blue lines) films, cast from (a) chloroform and (b) toluene. In both (a and b), the PL spectra are collected at room temperature, with a gate-width of 10 ns, 10 ns after photoexcitation. For clarity the PL intensity of the spectral region between 358–511 nm is multiplied by a factor of 15. Time-integrated PL spectra of PF26:PtOEP 6 wt% (black lines-squares) and PFO:PtOEP 6 wt% (blue lines-squares) films, cast from (c) chloroform and (d) toluene. In both (c and d) the data are collected at room temperature and corrected for the absorptance ($1 - T$) of the films at the photoexcitation at 532 nm, in resonance with the Q-absorption band of the PtOEP annihilator/sensitizer.

Clearly for the films developed by toluene (Fig. 3b), the PFO:PtOEP 6 wt% film exhibits a four-time stronger TTA-UC PL signal than the PF26:PtOEP 6 wt% film. In contrast, both systems developed by chloroform (Fig. 3a) exhibit a comparable TTA-UC PL intensity. The spectral shape of the TTA-UC PL signal of the toluene-based PFO:PtOEP 6 wt% film is spectrally-narrower than the corresponding TTA-UC PL signal of the toluene-based PF26:PtOEP 6 wt% film. In addition, the maximum PL intensity centers at around 440 nm corresponding to the $S_{0-0} \leftarrow S_{1-0}$ and it is red-shifted in respect to the respective PL intensity of the PF26:PtOEP 6 wt% film. The observed spectral narrowing and red-shift, in combination with the characteristic UV-Vis absorption feature observed at 435 nm verify the positive impact of the toluene solvent on the formation of the PFO β-phase backbone conformation (ESI†) and the consequent enhancement of the TTA-UC PFO luminescence intensity in this film. A similar observation is made in the time-integrated mode, when a band pass filter is used for registering the up-converted luminescence of the studied films. For the PFO:PtOEP film cast from toluene, the lower transmittance of the band pass filter in the spectral region at 460 nm reduces the relative PL intensity of the 0–1 vibronic emission peak in respect to the 0–0 peak. Nonetheless, the time-integrated PL spectra of the PF:PtOEP films shown in Fig. 3c and d are in good agreement with the corresponding time-gated PL spectra, confirming the positive impact of the PFO β-phase formation on the produced TTA-UC luminescence intensity. Fig. 3d shows that the maximum TTA-UC PL signal is obtained by the toluene-cast PFO:PtOEP 6 wt% film that delivers a nearly four-time stronger TTA-UC PL intensity than the rest of the films studied. For this system, the maximum TTA-UC PL intensity of the $S_{0-0} \leftarrow S_{1-0}$ transition is found at around 440 nm where the β-phase PFO species emit.

Fig. 4a and b present the photoexcitation dependence of the time-integrated TTA-UC PL signal of the PFO:PtOEP 6 wt% and PF26:PtOEP 6 wt% films developed by chloroform (Fig. 4c) and by toluene (Fig. 4b). The photoexcitation dependence of the time-integrated PtOEP phosphorescence intensity of these films and of their corresponding PS:PtOEP 6 wt% references is also displayed.

In all cases, the TTA-UC PL signal of the PFO:PtOEP 6 wt% and PF26:PtOEP 6 wt% systems becomes detectable at photoexcitation intensities higher than 100 μJ $pulse^{-1}$ (2.5 mW cm^{-2}); that is the photoexcitation regime where the PtOEP phosphorescence starts to depend sub-linearly on photoexcitation intensity. This observation verifies that the TTA-UC PL signal in the studied systems is activated by the annihilation of triplet-excited PtOEP sensitizers, as described in the generic mechanism displayed in Fig. 1; a TTA-induced doubly photoexcited state in PtOEP feeds the singlet state manifold of the PF matrices and results in green-to-blue TTA-UC luminescence of the PF matrices. What's more, in respect to the PtOEP

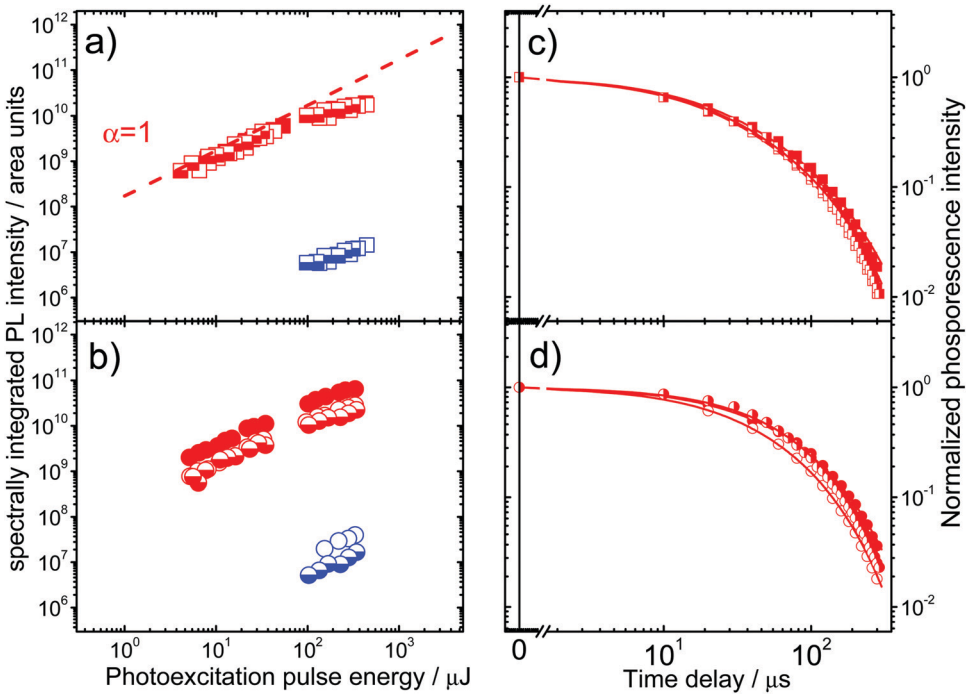

Fig. 4 Room temperature photoexcitation dependence of spectrally integrated PtOEP phosphorescence (red symbols) and of TTA-UC luminescence (blue symbols) of (a) chloroform-cast films of PS:PtOEP 6 wt% (filled squares), PFO:PtOEP 6 wt% (open squares) and PF26:PtOEP 6 wt% (semi-filled squares) and (b) toluene-cast films of PS:PtOEP 6 wt% (filled circles), PFO:PtOEP 6 wt% (open circles) and PF26:PtOEP 6 wt% (semi-filled circles) composites. In both (a and b) a correction is applied for the absorptance ($1 - T$) of the films at the excitation wavelength (λ_{exc} = 532 nm). Normalized time-gated PtOEP phosphorescence kinetics of (c) chloroform-cast films of PS:PtOEP 6 wt% (filled squares), PFO:PtOEP 6 wt% (open squares) and PF26:PtOEP 6 wt% (semi-filled squares), and (d) toluene-cast films of PS:PtOEP 6 wt% (filled circles), PFO:PtOEP 6 wt% (open circles) and PF26:PtOEP 6 wt% (semi-filled circles). The solid lines in (c and d) correspond to fits on the data based on eqn (2).

phosphorescence intensity of the PS:PtOEP 6 wt% reference systems, the PtOEP phosphorescence of the PFO:PtOEP 6 wt% and PF26:PtOEP 6 wt% films is practically the same, underlining a negligible PtOEP phosphorescence quenching and ruling out the occurrence of TET events from PtOEP sensitizer to the PF activators. Finally, only for the case of the toluene-cast films the intensity of the PFO:PtOEP 6 wt% TTA-UC PL signal is about three times stronger than the corresponding PL intensity of the PF26:PtOEP 6 wt% blend film, verifying the positive impact of the β-phase PFO formation on the process of TTA-UC PL generation. It worth noting that in respect to the glassy PFO solid-state samples, β-phase PFO films can exhibit a maximum PLQY improvement in the order of 30%.[36] Therefore, the herein observed 3×–4× enhancement in TTA-UC PL intensity cannot be attributed to differences in the PLQY values of the PFO luminescence between the two PFO:PtOEP blends processed by toluene and chloroform. The time-gated PL kinetics of the TTA-UC signal found an average TTA-UC PL lifetime in the order of 100 ns (ESI†).

Having ensured that the TTA-UC PL signal of these systems involves the annihilation of PtOEP triplet excited states we can now describe the rate law for the consumption of the PtOEP triplet excitons, in the photoexcitation intensity regime where TTA-UC is observed. This rate law is best described by eqn (1).[17,37]

$$\frac{d[T_1]}{dt} = -k_{obs}[T_1] - \gamma_{TTA\_PtOEP}[T_1]^2, \quad (1)$$

Here, $k_{obs} = (k_r + k_{nr}) = \frac{1}{\tau_{Ph}}$ corresponds to the inverse observable PtOEP phosphorescence lifetime τ_{Ph} with k_r and k_{nr} to describe the radiative and non-radiative monomolecular rate constant respectively, whereas γ_{TTA_PtOEP} corresponds to the bimolecular rate constant of the PtOEP triplet excitons. The analytic solution of eqn (1) provides the integrated rate law of the PtOEP triplet excited state kinetics and it is given by eqn (2).

$$[T_1]_t = \frac{[T_1]_0}{\left(1 + [T_1]_0 \frac{\gamma_{TTA\_PtOEP}}{k_{obs}}\right) e^{tk_{obs}} - [T_1]_0 \frac{\gamma_{TTA\_PtOEP}}{k_{obs}}}, \quad (2)$$

Fig. 4c and d present the normalized PtOEP phosphorescence dynamics of the PS:PtOEP 6 wt%, PFO:PtOEP 6 wt% and PF26:PtOEP 6 wt% blend films as developed by chloroform (Fig. 4c) and by toluene (Fig. 4d), after photoexcitation of the films at 532 nm with a pulse energy of 290 μJ. Table 1 summarizes the determined values of τ_{Ph} and γ_{TTA_PtOEP} for each of the systems studied after fitting of the time-gated PtOEP phosphorescence dynamics with eqn (2). Taking into account the effective molecular radius of PtOEP (r = 8.7 Å),[38] the diffusion coefficient $D_{T_1\_PtOEP}$ of the PtOEP triplet exciton in each system can be derived from the relationship $\gamma_{TTA\_PtOEP} = 8\pi R D_{T_1\_PtOEP}$, where $R = 2r$ corresponds to the center-to-center distance of the two annihilating triplet PtOEP excitons. For all systems, the obtained $D_{T_1\_PtOEP}$ values are in the order of 10^{-9} cm^2 s^{-1}. This parameter informs about the diffusivity of the PtOEP triplet exciton, and it is in an excellent agreement with the previous reported value of 6×10^{-9} cm^2 s^{-1} found for blends of PtOEP:Alq$_3$.[39] On the basis of the determined PtOEP phosphorescence lifetimes, the percentage quenching efficiency (Φ_q) of the PtOEP phosphorescence in the PF-based blends of PFO:PtOEP 6 wt% and PF26:PtOEP 6 wt%, was calculated by eqn (3).

$$\Phi_q = 100 \times \left(1 - \frac{\tau_{Ph\text{-}PF:PtOEP}}{\tau_{Ph\text{-}PS:PtOEP}}\right), \quad (3)$$

For both solvents used, the calculated Φ_q values are found comparable, in the order of 20%. Since no TET is possible from the triplet-excited PtOEP sensitizer to the PF matrices, the observed PtOEP phosphorescence quenching is attributed to the different extent of TTA events in the PtOEP phase that in turn depends on the different degree of PtOEP aggregation in each system. Interestingly, the highest phosphorescence quenching efficiency is found for the toluene-cast PF26:PtOEP 6 wt% blend film that exhibits the highest value of the γ_{TTA_PtOEP} constant, in the order of 10^{-13} cm^3 s^{-1}. Indeed, the time-gated PL spectrum of the PF26:PtOEP 6 wt% film developed by toluene (Fig. 3b) exhibits enhanced PL intensity in the spectral region between 560–580 nm, where the TTA-induced PtOEP delayed fluorescence signal is expected, and this feature disappears within 50 ns after photoexcitation (ESI†). For the rest of the studied films, the determined values of the bimolecular rate constant γ_{TTA_PtOEP} are found comparable in the order of 10^{-14} cm^3 s^{-1}. Future time-resolved PL characterization measurements of the PS:PtOEP, PFO:PtOEP and PF26:PtOEP composite systems in the ps–ns time scale are expected to provide useful information for addressing the relationship between the quenching efficiency of the PtOEP delayed fluorescence and the energy transfer efficiency from a doubly photoexcited PtOEP state to the PF matrices. Table 1 informs that the β-phase-containing PFO:PtOEP 6 wt% blend film spun from toluene exhibits a relatively low triplet-exciton bimolecular rate constant, $\gamma_{TTA\_PtOEP} = 1.8 \times 10^{-14}$ cm^3 s^{-1}, yet it possesses the

Table 1 Overview of the fitting results obtained by using eqn (2) for fitting the time-gated PtOEP phosphorescence dynamics of all systems studied in this work. Based on the determined time constants τ_{Ph}, the percentage quenching efficiency Φ_q of the PtOEP phosphorescence lifetime was calculated with eqn (3). The calculated value of the triplet PtOEP exciton diffusion coefficient $D_{T_1\_PtOEP}$ is also reported for each system

System	τ_{Ph} (μs)	Φ_q (%)	γ_{TTA_PtOEP} (cm^3 s^{-1})	$D_{T_1\_PtOEP}$ (cm^2 s^{-1})
PS:PtOEP 6 wt% from $CHCl_3$	128 ± 4	—	$1.1 \times 10^{-14} \pm 2.4 \times 10^{-15}$	$2.5 \times 10^{-9} \pm 5.5 \times 10^{-10}$
PFO:PtOEP 6 wt% from $CHCl_3$	100 ± 2	21 ± 5	$1.4 \times 10^{-14} \pm 2.9 \times 10^{-15}$	$3.2 \times 10^{-9} \pm 6.6 \times 10^{-10}$
PF26:PtOEP 6 wt% from $CHCl_3$	106 ± 3	17 ± 5	$1.8 \times 10^{-14} \pm 2.7 \times 10^{-15}$	$4.1 \times 10^{-9} \pm 6.2 \times 10^{-10}$
PS:PtOEP 6 wt% from toluene	117 ± 3	—	$3.8 \times 10^{-14} \pm 1.8 \times 10^{-14}$	$8.7 \times 10^{-9} \pm 4.1 \times 10^{-9}$
PFO:PtOEP 6 wt% from toluene	92 ± 1	21 ± 3	$1.8 \times 10^{-14} \pm 4.6 \times 10^{-15}$	$4.1 \times 10^{-9} \pm 1.1 \times 10^{-9}$
PF26:PtOEP 6 wt% from toluene	88 ± 1	25 ± 2	$1.1 \times 10^{-13} \pm 6.7 \times 10^{-15}$	$2.5 \times 10^{-8} \pm 1.5 \times 10^{-9}$

most planarized PF backbone conformation thereby delivering the highest TTA-UC PL signal intensity. Consequently, we can suggest that the efficiency of the energy transfer step from doubly excited PtOEP to the PF matrices primarily depends on the availability of planarized PF activator conformers and not on the diffusivity of the PtOEP triplet excitons in the PtOEP phase.

Next, we performed temperature-dependent time-integrated PL characterization measurements on both sets of the PFO:PtOEP 6 wt% and PF26:PtOEP 6 wt% samples, in the temperature range of 100–290 K. The relative TTA-UC PL efficiency of the PFO:PtOEP 6 wt% and PF26:PtOEP 6 wt% blend films is displayed in Fig. 5a and b, respectively. In addition, the relative PtOEP phosphorescence efficiency of these films is presented in Fig. 5c and d. Regardless of the solvent and the side-chains of the PF matrix used, we find that by lowering the temperature the relative efficiency of the TTA-UC PL signal increases, exhibiting a two-time stronger TTA-UC PL intensity at 100 K. Interestingly, the magnitude of the step change observed in the TTA-UC PL signal in each film is inversely proportional to the magnitude of the step change observed in the corresponding PtOEP phosphorescence intensity. By lowering the temperature, the increase of the TTA-UC PL intensity becomes steeper as the rise of the PtOEP phosphorescence intensity starts to decelerate.

The observed enhancement of the TTA-UC PL intensity of the PFO:PtOEP 6 wt% and PF26:PtOEP 6 wt% films at lower temperatures indicates that no energy barrier needs to be surpassed[40] for generating TTA-UC luminescence in these systems, providing additional solid evidence that no endothermic energy transfer process from triplet excited PtOEP to the PF matrices takes place.

The observed temperature dependence of the TTA-UC PL intensity is very similar to that previously seen in solid-state TTA-UC composites where the TTA-UC process is driven by exothermic triplet energy transfer steps between sensitizer and activator.[16,17] The common temperature dependent character of the TTA-UC process in the two different classes of TTA-UC solid-state composites should be linked primarily to the temperature dependence of the PtOEP triplet exciton diffusion process. The detailed description of the triplet exciton diffusivity in solid TTA-UC composites as a function of temperature is beyond the scope of this work. We note however that previous dielectric spectroscopy studies have set the glass transition temperature of the PF homopolymer to ~60 °C.[41] At temperatures lower than room temperature, any segmental motion that could potentially assist translational mobility of the PtOEP component in the PF:PtOEP blends can be ruled out, and triplet exciton diffusion should be considered as a result of energy migration[42] and/or energy transfer.[9,43] Practically, in solid-state TTA-UC composites the effect of lowering the temperature: (i) removes all non-radiative channels that deactivate triplet-excited states (ii) slows down the diffusion of triplet excitons, thereby decelerating TTA events and reducing trapping of triplet excitons to sites that act as energy scavengers (*e.g.* aggregates)

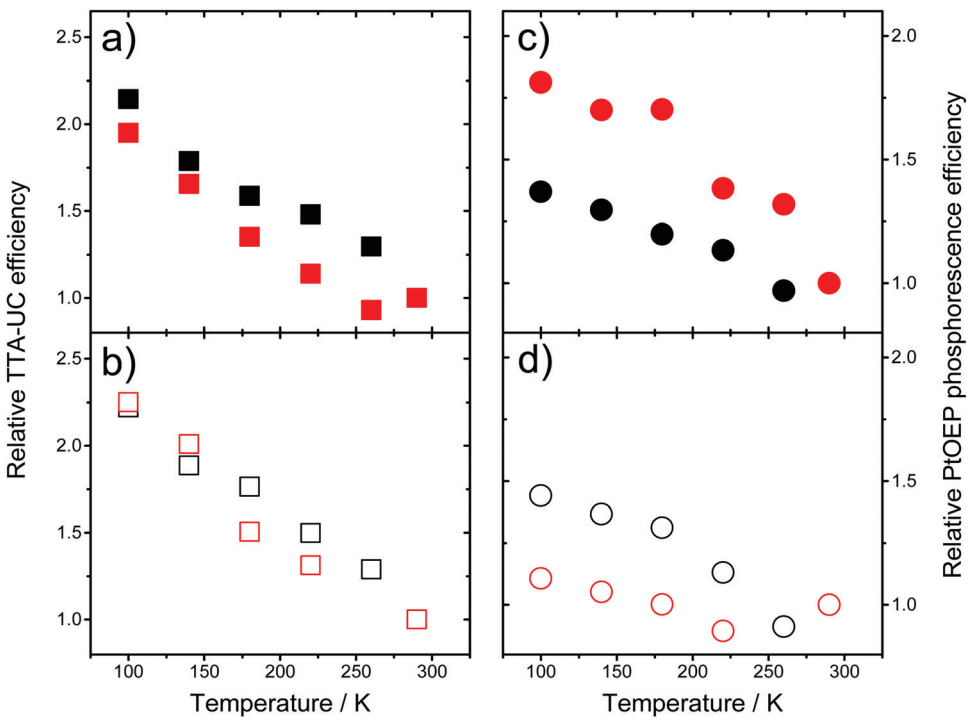

Fig. 5 The relative efficiency of the green-to-blue PF TTA-UC PL intensity, as a function of temperature for (a) PFO:PtOEP 6 wt% films cast from chloroform (black-filled squares) and toluene (red-filled squares) and (b) PF26:PtOEP 6 wt% films cast from chloroform (black-open squares) and toluene (red-open squares). The relative efficiency of the PtOEP phosphorescence intensity, as a function of temperature for (c) PFO:PtOEP 6 wt% films cast from chloroform (black-filled circles) and toluene (red-filled circles) and (d) PF26:PtOEP 6 wt% films cast from chloroform (black-open circles) and toluene (red-open circles). In all cases the films were photoexcited at 532 nm, in resonance with the Q-absorption band of the PtOEP annihilator/sensitizer.

(iii) impedes triplet exciton de-trapping from relatively shallow energy trapping sites. As such, the overall effect of lowering the temperature on the phosphorescence and the TTA-UC PL intensities is hardly described without carefully developing a theoretical microscopic model.

In order to demonstrate unequivocally that no triplet energy transfer occurs from triplet-excited PtOEP to PFO, we have performed cw-PIA spectroscopic experiments[44] in PFO-only, PF26-only, PFO:PtOEP 6 wt% and PF26:PtOEP 6 wt% blend films. In the event of triplet energy transfer from PtOEP to PFO, the characteristic PIA band of the $T_1 \rightarrow T_n$ transition in the PF matrix[31] should be observed, in the spectral region of 830 nm. Indeed, Fig. 6a shows that this spectral feature is present in the cw-PIA spectra of PFO-only and PF26-only films cast from toluene and chloroform, when PF is resonantly photoexcited at 405 nm. However, no detection of this PIA spectral feature is possible when PFO:PtOEP and PF26:PtOEP films are photoexcited at 532 nm where PtOEP only absorbs. The overview of the corresponding cw-PIA spectra displayed in Fig. 6 confirms the absence of triplet energy transfer from triplet-excited PtOEP to the PF derivatives.

Considering the singlet and triplet energy levels of the PF and PtOEP, the energy diagram shown in Fig. 7 depicts how TTA in the PtOEP phase can lead to the activation of photon up-converted PF luminescence in the studied PF:PtOEP blends. The annihilation of two triplet PtOEP excitons results in the population of a doubly photoexcited state D* in PtOEP, which can facilitate the transfer of energy to the PF activator. The stronger up-converted PF luminescence that is observed in the PFO:PtOEP blends with a high β-phase PFO content, reflects

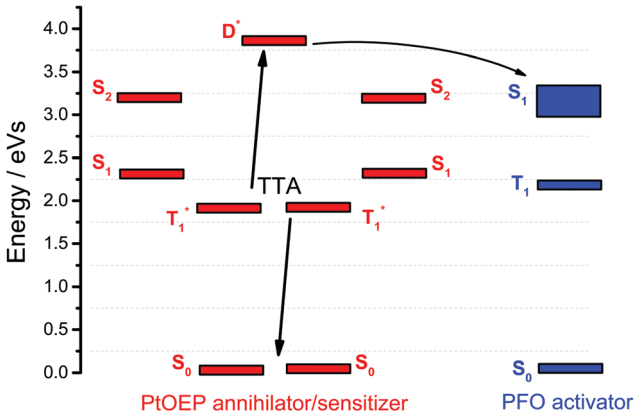

Fig. 7 The energy diagram of the PFO:PtOEP composite system depicting the energetics of the levels that are involved in the generation of green-to-blue TTA-UC luminescence.

the important role of planarized backbone conformations in the proposed energy transfer mechanism. In principle, the electron-exchange mediated photon up-conversion in this type of TTA-UC composites is influenced positively by the orbital overlap achieved *via* the electronic interaction of the doubly photoexcited PtOEP chromophore and the planarized PFO conformers.[24] The observation of delayed fluorescence in PtOEP after photoexcitation at 532 nm[17] suggests that the D* state can alternatively undergo a transition to the first singlet state of PtOEP ($D^* \rightarrow S_{1\_PtOEP}$). In case where the D* and S_{1_PtOEP} states have the same spin multiplicity, the $D^* \rightarrow S_{1\_PtOEP}$ transition corresponds to an internal conversion and it should

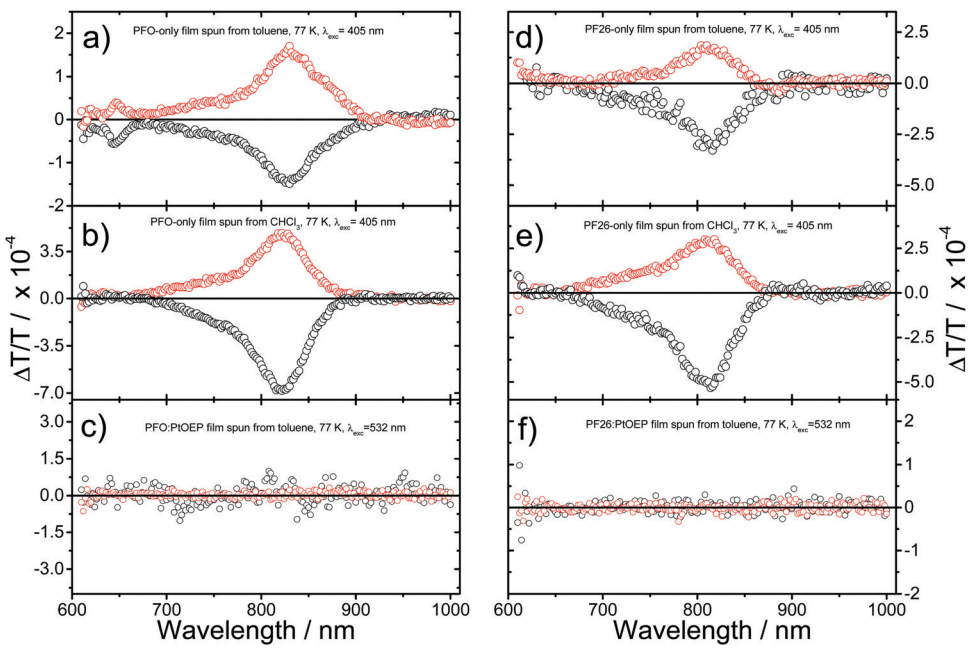

Fig. 6 PIA spectra as registered at 77 K for a layer of (a) PFO-only film spun from toluene, (b) PFO-only film spun from chloroform, (c) PFO:PtOEP blend film spun from toluene, (d) PF26-only film spun from toluene, (b) PF26-only film spun from chloroform, (c) PF26:PtOEP blend film spun from toluene. The excitation modulation frequency is 80 Hz. For the measurements on single-component films, the excitation laser wavelength is 405 nm, with the intensity of 15 mW cm^{-2}. While for the measurements on blend films, the excitation laser wavelength is 532 nm, with the intensity of 46 mW cm^{-2}.

be rapid. Therefore, when planarized PFO conformers are available, the proposed energy transfer step from D* to PFO must occur with a rate comparable to, or higher than the rate of the competing $D^* \rightarrow S_{1\_PtOEP}$ relaxation. The response of the PF26:PtOEP film demonstrates that even when the diffusivity of the PtOEP triplet excitons is high (*i.e.* film cast from toluene, see Table 1), the absence of planar PF26 conformers favours the antagonistic $D^* \rightarrow S_{1\_PtOEP}$ deactivation channel, and delayed PtOEP fluorescence is produced on the expense of the TTA-UC PL intensity.

Our findings offer the opportunity to discuss about a potential link between exciton fission and fusion that operate in organic systems. The origin of the TTA-induced doubly photoexcited state D* in PtOEP was recently addressed,[25] nonetheless further studies could be performed to fully decipher its nature. Considering recent findings about singlet exciton fission,[45–47] it is reasonable to speculate that TTA reactions in PtOEP could activate an intermediate triplet-pair state $(TT)_1$ in which photon energy can be stored and utilized. Future experiments should clarify whether the TTA-driven doubly photoexcited state of PtOEP corresponds to a $(TT)_1$ state that can undergo heteroatomic inverse intersystem crossing[48] to the first singlet-excited state of the planarized PFO activator.

Conclusions

In conclusion, we have presented a spectroscopic study of solution-processable thin films prepared by the unconventional TTA-UC composite of PFO:PtOEP. In this system, photon energy up-conversion proceeds *via* TTA reactions in the phase of the green-absorbing PtOEP triplet sensitizer enabling the generation of blue up-converted PFO luminescence. No exothermic triplet energy transfer takes place between triplet-excited PtOEP and ground state PFO, as verified by cw-PIA spectroscopy. Instead, TTA reactions in the PtOEP phase activate a doubly photoexcited PtOEP state from where energy is transferred to PFO for producing the TTA-UC luminescence. The intensity of the observed green-to-blue TTA-UC luminescence becomes stronger when the molecular conformation of the PFO matrix is tuned to the planarized β-phase by a simple solution-based processing protocol.

The capability of storing electronic energy in a higher lying excited state *via* exciton spin management offers a string of new possibilities relevant to technologically important applications. Beyond state-of-the-art photonic applications can be developed to enable confocal-based high spatial resolution spectral imaging, and near-field scanning optical microscope-based experiments that operate in the TTA-UC mode. By utilizing the property of the PFO:PtOEP blends to exhibit dual spectral shape in their TTA-UC signal response, an optical probe can be established for determining the local PFO molecular conformation in inhomogeneous PFO films. Alternatively, PFO:PtOEP blend films with known β-phase PFO content can be used in applications where sharp contrast in the optical properties of adjacent spot areas is desired so that efficient TTA-UC-based photonic switches[49] and organic TTA-UC metamaterials[50] can be obtained. Moreover, the important role of PF backbone conformation in the spectral properties of this type of TTA-UC systems can be used for tuning on-demand the response of upconverted circularly polarized luminescence.[51–53]

Essentially, the proposed mechanism for TTA-UC generation provides generic guidelines for a simple protocol to develop low-cost and easily processable TTA-UC polymeric coating platforms. Storage of photon energy can be enabled by properly designed triplet annihilator/sensitizer species, after engineering their tendency to segregate. Harvesting the stored photon energy from these systems can be achieved by acceptors of appropriate molecular conformation. The implications of the proposed strategy are of importance considering the emergence of several contemporary molecular architectures that facilitate singlet–triplet intersystem crossing steps without the need for a heavy atom in their molecular structure.

Conflicts of interest

There are no conflicts to declare.

Acknowledgements

P. E. K. acknowledges the financial support of a start-up grant from Cyprus University of Technology. S. L. and J. S. K. thank the UK ESPRC for the Plastic Electronics Centre for Doctoral Training (EP/L016702/1) funding. C.-G. acknowledges financial support from the Spanish Ministry of Economy and Competitiveness through projects MAT2014-57652-C2-1/2-R (LAPSEN) and PCIN-2015-169-C02-01/02 (MOFSENS) and through the Severo Ochoa Programme for Centers of Excellence (SEV-2016-0686) and the Campus of International Excellence (CEI) UAM+CSIC.

References

1 A. C. Somersall and J. E. Guillet, *Macromolecules*, 1973, **6**, 218–223.
2 D. Hertel and H. Bässler, *J. Chem. Phys.*, 2001, **115**, 10007.
3 C. Rothe and A. Monkman, *J. Chem. Phys.*, 2005, **123**, 244904.
4 C. A. Parker and C. G. Hatchard, *Proc. Chem. Soc., London*, 1962, 386–387.
5 D. V. Kozlov and F. N. Castellano, *Chem. Commun.*, 2004, 2860–2861.
6 F. Laquai, G. Wegner, C. Im, A. Buesing and S. Heun, *J. Chem. Phys.*, 2005, **123**, 074902.
7 S. Baluschev, T. Miteva, V. Yakutkin, G. Nelles, A. Yasuda and G. Wegner, *Phys. Rev. Lett.*, 2006, **97**, 143903.
8 S. Baluschev, V. Yakutkin, G. Wegner, B. Minch, T. Miteva, G. Nelles and A. Yasuda, *J. Appl. Phys.*, 2007, **101**, 023101.
9 A. Monguzzi, R. Tubino and F. Meinardi, *Phys. Rev. B: Condens. Matter Mater. Phys.*, 2008, **77**, 155122.
10 T. N. Singh-Rachford and F. N. Castellano, *Coord. Chem. Rev.*, 2010, **254**, 2560–2573.

11 V. Gray, K. Moth-Poulsen, B. Albinsson and M. Abrahamsson, *Coord. Chem. Rev.*, 2018, **362**, 54–71.
12 S. Raišys, K. Kazlauskas, S. Juršėnas and Y. C. Simon, *ACS Appl. Mater. Interfaces*, 2016, **8**, 15732–15740.
13 T. Ogawa, M. Hosoyamada, B. Yurash, T.-Q. Nguyen, N. Yanai and N. Kimizuka, *J. Am. Chem. Soc.*, 2018, **140**, 8788–8796.
14 S. Raišys, S. Juršėnas, Y. C. Simon, C. Weder and K. Kazlauskas, *Chem. Sci.*, 2018, **9**, 6796–6802.
15 V. Jankus, E. W. Snedden, D. W. Bright, V. L. Whittle, J. A. G. Williams and A. Monkman, *Adv. Funct. Mater.*, 2013, **23**, 384–393.
16 H. Goudarzi and P. E. Keivanidis, *J. Phys. Chem. C*, 2014, **118**, 14256–14265.
17 H. Goudarzi and P. E. Keivanidis, *ACS Appl. Mater. Interfaces*, 2017, **9**, 845–857.
18 P. E. Keivanidis, S. Baluschev, T. Miteva, G. Nelles, U. Scherf, A. Yasuda and G. Wegner, *Adv. Mater.*, 2003, **15**, 2095–2098.
19 S. Baluschev, P. E. Keivanidis, G. Wegner, J. Jacob, A. C. Grimsdale, K. Müllen, T. Miteva, A. Yasuda and G. Nelles, *Appl. Phys. Lett.*, 2005, **86**, 061904.
20 S. Baluschev, J. Jacob, Y. S. Avlasevich, P. E. Keivanidis, T. Miteva, A. Yasuda, G. Nelles, A. C. Grimsdale, K. Müllen and G. Wegner, *ChemPhysChem*, 2005, **6**, 1250–1253.
21 J. Zhou, Q. Liu, W. Feng, Y. Sun and F. Li, *Chem. Rev.*, 2015, **115**, 395–465.
22 L. Frazer, J. K. Gallaher and T. W. Schmidt, *ACS Energy Lett.*, 2017, **2**, 1346–1354.
23 P. E. Keivanidis, S. Baluschev, G. Lieser and G. Wegner, *ChemPhysChem*, 2009, **10**, 2316–2326.
24 P. E. Keivanidis, F. Laquai, J. W. F. Robertson, S. Baluschev, J. Jacob, K. Müllen and G. Wegner, *J. Phys. Chem. Lett.*, 2011, **2**, 1893–1899.
25 J. A. Hinke, T. J. Pundsack, W. A. Luhman, R. J. Holmes and D. A. Blank, *J. Chem. Phys.*, 2013, **139**, 101102.
26 S. K. Sugunan, U. Tripathy, S. M. Brunet, M. F. Paige and R. P. Steer, *J. Phys. Chem. A*, 2009, **113**, 8548–8556.
27 V. Gray, K. Börjesson, D. Dzebo, M. Abrahamsson, B. Albinsson and K. Moth-Poulsen, *J. Phys. Chem. C*, 2016, **120**, 19018–19026.
28 S. Bagnich and H. Bässler, *Chem. Phys. Lett.*, 2003, **381**, 464–470.
29 R. Huang, J. S. Ward, N. A. Kukhta, J. Avó, J. Gibson, T. Penfold, J. C. Lima, A. S. Batsanov, M. N. Berberan-Santos, M. R. Bryce and F. B. Dias, *J. Mater. Chem. C*, 2018, **6**, 9238–9247.
30 M. Grell, D. D. C. Bradley, G. Ungar, J. Hill and K. S. Whitehead, *Macromolecules*, 1999, **32**, 5810–5817.
31 C. Rothe, S. M. King, F. Dias and A. P. Monkman, *Phys. Rev. B: Condens. Matter Mater. Phys.*, 2004, **70**, 195213.
32 A. L. T. Khan, M. J. Banach and A. Köhler, *Synth. Met.*, 2003, **139**, 905–907.
33 M. Arif, C. Volz and S. Guha, *Phys. Rev. Lett.*, 2006, **96**, 025503.
34 C. Volz, M. Arif and S. Guha, *J. Chem. Phys.*, 2007, **126**, 064905.
35 W. C. Tsoi and D. G. Lidzey, *J. Phys.: Condens. Matter*, 2008, **20**, 125213.
36 A. Perevedentsev, N. Chander, J.-K. Kim and D. D. C. Bradley, *J. Polym. Sci., Part B: Polym. Phys.*, 2016, **54**, 1995–2006.
37 B. H. Wallikewitz, D. Kabra, S. Gelinas and R. H. Friend, *Phys. Rev. B: Condens. Matter Mater. Phys.*, 2012, **85**, 045209.
38 A. Bondi, *J. Phys. Chem.*, 1964, **68**, 441–451.
39 M. A. A. Baldo, C. Adachi and S. R. Forrest, *Phys. Rev. B: Condens. Matter Mater. Phys.*, 2000, **62**, 10967.
40 P. Atkins and J. de Paula, *Physical Chemistry*, Macmillan Education, 9th edn, 2010.
41 P. Papadopoulos, G. Floudas, C. Chi and G. Wegner, *J. Chem. Phys.*, 2004, **120**, 2368–2374.
42 A. Köhler and H. Bässler, *Mater. Sci. Eng., R*, 2009, **66**, 71–109.
43 W. Staroske, M. Pfeiffer, K. Leo and M. Hoffmann, *Phys. Rev. Lett.*, 2007, **98**, 197402.
44 C.-L. Lee, X. Yang and N. C. Greenham, *Phys. Rev. B: Condens. Matter Mater. Phys.*, 2007, **76**, 245201.
45 Y. Tamai, H. Ohkita, H. Benten and S. Ito, *J. Phys. Chem. C*, 2013, **117**, 10277–10284.
46 S. Lukman, J. M. Richter, L. Yang, P. Hu, J. Wu, N. C. Greenham and A. J. Musser, *J. Am. Chem. Soc.*, 2017, **139**, 18376–18385.
47 C. K. Yong, A. J. Musser, S. L. Bayliss, S. Lukman, H. Tamura, O. Bubnova, R. K. Hallani, A. Meneau, R. Resel, M. Maruyama, S. Hotta, L. M. Herz, D. Beljonne, J. E. Anthony, J. Clark and H. Sirringhaus, *Nat. Commun.*, 2017, **8**, 15953.
48 C. Richter, W. Hub, R. Traber and S. Schneider, *Photochem. Photobiol.*, 1987, **45**, 671–673.
49 A. Perevedentsev, Y. Sonnefraud, C. R. Belton, S. Sharma, A. E. G. Cass, S. A. Maier, J.-K. Kim, P. N. Stavrinou and D. D. C. Bradley, *Nat. Commun.*, 2015, **6**, 5977.
50 G. Ryu, P. N. Stavrinou and D. D. C. Bradley, *Adv. Funct. Mater.*, 2009, **19**, 3237–3242.
51 M. Oda, H.-G. Nothofer, G. Lieser, U. Scherf, S. C. J. Meskers and D. Neher, *Adv. Mater.*, 2000, **12**, 362–365.
52 J. Li, X. Peng, C. Huang, Q. Qi, W.-Y. Lai and W. Huang, *Polym. Chem.*, 2018, **9**, 5278–5285.
53 X. Yang, J. Han, Y. Wang and P. Duan, *Chem. Sci.*, 2019, **10**, 172–178.